Subgrid-scale modeling of helicity and energy dissipation in helical turbulence

Yi Li,[1] Charles Meneveau,[1] Shiyi Chen,[1,2] and Gregory L. Eyink[3]
[1]*Department of Mechanical Engineering and Center for Environmental and Applied Fluid Mechanics, The Johns Hopkins University, Baltimore, Maryland 21218, USA*
[2]*COE and CCSE, Peking University, Beijing, 100871, People's Republic of China*
[3]*Department of Applied Mathematics and Statistics, The Johns Hopkins University, Baltimore, Maryland 21218, USA*
(Received 5 May 2006; published 30 August 2006)

The subgrid-scale (SGS) modeling of helical, isotropic turbulence in large eddy simulation is investigated by quantifying rates of helicity and energy cascade. Assuming Kolmogorov spectra, the Smagorinsky model with its traditional coefficient is shown to underestimate the helicity dissipation rate by about 40%. Several two-term helical models are proposed with the model coefficients calculated from simultaneous energy and helicity dissipation balance. The helical models are also extended to include dynamic determination of their coefficients. The models are tested *a priori* in isotropic steady helical turbulence. Together with the dynamic Smagorinsky model and the dynamic mixed model, they are also tested *a posteriori* in both decaying and steady isotropic helical turbulence by comparing results to direct numerical simulations (DNS). The *a priori* tests confirm that the Smagorinsky model underestimates SGS helicity dissipation, although quantitative differences with the predictions are observed due to the finite Reynolds number of the DNS. Also, in *a posteriori* tests improvement can be achieved for the helicity decay rate with the proposed models, compared with the Smagorinsky model. Overall, however, the effect of the new helical terms added to obtain the correct rate of global helicity dissipation is found to be quite small. Within the small differences, the various versions of the dynamic model provide the results closest to the DNS. The dynamic model's good performance in capturing mean kinetic energy dissipation at the finite Reynolds number of the simulations appears to be the most important aspect in accounting also for accurate prediction of the helicity dissipation.

DOI: 10.1103/PhysRevE.74.026310 PACS number(s): 47.27.Gs

I. INTRODUCTION

In turbulent flows, the importance of helicity, $h=\boldsymbol{u}\cdot\boldsymbol{\omega}$ (where $\boldsymbol{u}$ and $\boldsymbol{\omega}$ are the velocity and vorticity fields, respectively), originates from the facts that it is an inviscid invariant and it is related to the linkage of the vortex lines of the flow [1]. Many conjectures about the consequences of these two properties have been proposed. For example, it was conjectured that in helical turbulence with constant helicity injection, helicity would cascade from the injection scale to smaller scales [2]. Two possible pictures were proposed based on different assumptions: either the helicity cascade totally blocks the energy cascade, reminiscent of the dual energy and enstrophy cascades in two-dimensional turbulence, or it cascades linearly with energy like a passive scalar. These ideas were further analyzed and the latter picture was observed in the eddy-damped quasi-normal Markovian (EDQNM) model calculation [3] and direct numerical simulation (DNS) [4,5], while it was suggested [3,4,6] that the former picture was unlikely to be observed. It was also speculated that the invariance and topological nature of helicity would increase the probability of the flow being locally Beltramized and that regions with high relative helicity should be correlated with low energy dissipation rate and vice versa [7,8]. This speculation was supported by the DNS conducted by Pelz *et al.* [9] in plane Poiseuille and Taylor-Green vortex flows, but the DNS in homogeneous flows and channel flows with higher resolution [10,11] and experiments in several shear flows [12] found no obvious correlation between helicity distribution and energy dissipation, and no general tendency of Beltramization. The observation that helicity is related to the nonlinear term of the Navier-Stokes (NS) equation by the vector identity

$$|\boldsymbol{u}\cdot\boldsymbol{\omega}|^2+|\boldsymbol{u}\times\boldsymbol{\omega}|^2=|\boldsymbol{u}|^2|\boldsymbol{\omega}|^2 \tag{1}$$

inspired another idea that persistence of nonzero mean helicity would suppress the energy cascade and thus reduce energy dissipation [9], which also served as another support for the conjecture that regions with high relative helicity would coincide with regions of low dissipation rate and vice versa. The DNS of Polifke and Shtilman [13] confirmed that in homogeneous turbulent flows with strong initial helicity the rate of energy cascade was suppressed. The same trend was obtained in the DNS of thermal convection between two plates with different types of mean shear [14]. On the other hand Speziale [15] pointed out that only the solenoidal part of the Lamb vector contributed to the energy cascade, therefore low helicity levels would not necessarily imply high energy cascade or high energy dissipation.

In terms of applications, it has long been recognized that the spectral distribution of helicity is related to the α effect observed in magnetohydrodynamics [1]. It was first noted by Lilly [16] that supercell thunderstorms were characterized by high helicity. A simple Beltrami flow model was proposed for the supercell storm and it was argued that the noted stability of a supercell storm could be attributed to the fact that helicity suppresses energy dissipation. The effect of buoyant forcing on helicity generation was also investigated [14] and it was found that buoyant forcing tended to amplify the helicity fluctuations when the mean flow field was helical.

Considering the possible effects of helicity on the energy cascade and on turbulence structure, it is of interest to explore the effects of helicity on subgrid-scale (SGS) structure and SGS modeling in the context of large-eddy simulation (LES). Specifically, we present in this paper an analysis of

SGS modeling of helical turbulence and helicity dissipation. LES of helical turbulence was previously treated by Lautenschlager *et al.* [17], but no particular emphasis was placed on the SGS modeling of helicity dissipation. Here, by exploiting the methodology pioneered by Lilly [18], we first quantify the SGS helicity dissipation rate of the traditional Smagorinsky model, showing that the Smagorinsky model will tend to underpredict helicity dissipation rates under canonical conditions. SGS models are then proposed and model coefficients are determined by simultaneous energy and helicity dissipation balance, or using the dynamic approach based on multiscale filterings [19]. The models, as well as the dynamic Smagorinsky model and the dynamic two-coefficient nonlinear model, are tested *a priori* and/or *a posteriori* in isotropic turbulence, and conclusions are presented.

II. THEORETICAL ANALYSIS

A. SGS helicity dissipation rate produced by the Smagorinsky model

From the NS equation one can derive the equation for the ensemble averaged helicity $\langle h\rangle \equiv \langle \boldsymbol{u}\cdot\boldsymbol{\omega}\rangle$,

$$\partial_t\langle h\rangle + \partial_j\langle u_j h\rangle = \partial_j\langle Q_j\rangle - 4\nu\langle S_{ij}\rangle\langle R_{ij}\rangle - \eta + 2\langle f_i\omega_i\rangle, \quad (2)$$

in which S_{ij} is the strain rate tensor and R_{ij} is the symmetric vorticity gradient tensor defined as $R_{ij}\equiv\frac{1}{2}(\partial_j\omega_i+\partial_i\omega_j)$. $\eta \equiv 4\nu\langle S'_{ij}R'_{ij}\rangle$ is the helicity dissipation rate with $S'_{ij}\equiv S_{ij}-\langle S_{ij}\rangle$, $R'_{ij}\equiv R_{ij}-\langle R_{ij}\rangle$. f_i is the forcing term in the NS equation, while Q_j is the flux term:

$$Q_j \equiv -\frac{p}{\rho}\omega_j + \frac{1}{2}u_iu_i\omega_j + 2\nu u_iR_{ij} + 2\nu\omega_iS_{ij} - \varepsilon_{jkm}u_kf_m. \quad (3)$$

In LES, one defines the resolved helicity as $h_\Delta \equiv \tilde{\boldsymbol{u}}\cdot\tilde{\boldsymbol{\omega}}$, with the wide tilde denoting filtered quantity at scale Δ. The equation for h_Δ can be derived from the filtered NS equation as

$$\partial_t h_\Delta + \partial_j(\tilde{u}_j h_\Delta) = \partial_j\tilde{Q}_j - \Pi_H - 4\nu\tilde{S}_{ij}\tilde{R}_{ij} + 2\tilde{f}_i\tilde{\omega}_i, \quad (4)$$

where $\Pi_H \equiv -2\tau_{ij}\tilde{R}_{ij}$ on the right-hand side (rhs) is the SGS helicity dissipation rate, with $\tau_{ij}\equiv\widetilde{u_iu_j}-\tilde{u}_i\tilde{u}_j$ being the SGS stress, and

$$\tilde{Q}_j \equiv -2\tilde{\omega}_i\tau_{ij} - \varepsilon_{ijk}\tilde{u}_i\partial_l\tau_{kl} - \tilde{\omega}_j\frac{\tilde{p}}{\rho} + \tilde{\omega}_j\frac{\tilde{u}_i\tilde{u}_i}{2} + 2\nu\tilde{R}_{ij}\tilde{u}_i + 2\nu\tilde{S}_{ij}\tilde{\omega}_i - \varepsilon_{jkm}\tilde{u}_k\tilde{f}_m \quad (5)$$

is the spatial flux term.

In helical isotropic turbulence, the spectral energy density tensor can be written as [4,20–22]

$$\Theta_{ij}(\mathbf{k},t) \equiv \langle\hat{u}_i^*(\mathbf{k},t)\hat{u}_j(\mathbf{k},t)\rangle = \frac{E(k,t)}{4\pi k^2}\left(\delta_{ij}-\frac{k_ik_j}{k^2}\right) + \iota\varepsilon_{ijl}\frac{k_l}{k^2}\frac{H(k,t)}{8\pi k^2}, \quad (6)$$

in which $\iota=\sqrt{-1}$ and $E(k)$ and $H(k)$ are the (radial) energy and helicity spectra (for simplicity, the dependence on time has been omitted). In the inertial range

$$E(k) = c_K\epsilon^{2/3}k^{-5/3}. \quad (7)$$

As proposed by Brissaud *et al.* [2] and confirmed by both the DNS with hyperviscosity [4] and with normal viscosity [5], in helical turbulence where there is constant helicity injection, the injected helicity will cascade to small scales where it is dissipated. This process yields, in the inertial range, a helicity spectrum of the form

$$H(k) = c_H\eta\epsilon^{-1/3}k^{-5/3}, \quad (8)$$

where the coefficient c_H was found to be approximately 1.0 [4]. Therefore in LES of helical turbulence where helicity plays an important role, one is interested in capturing accurately the SGS helicity dissipation, in addition to SGS energy dissipation which must be captured accurately in both helical and nonhelical turbulence.

Useful insight into this problem can be obtained by considering the ensemble averaged balance equation for the resolved helicity h_Δ, generalizing the method first applied by Lilly [18] to calculate the Smagorinsky coefficient. Consider homogeneous steady turbulence. Taking the ensemble average of Eq. (4) we obtain

$$-2\langle\tau_{ij}\tilde{R}_{ij}\rangle + 4\nu\langle\tilde{S}_{ij}\tilde{R}_{ij}\rangle = 2\langle\tilde{f}_i\tilde{\omega}_i\rangle. \quad (9)$$

Comparing this equation with Eq. (2), which in homogeneous steady turbulence reduces to the balance between helicity dissipation and helicity injection rate $\eta=2\langle f_i\omega_i\rangle$, and assuming that the filter size Δ is well inside the inertial range where the effects of viscosity and forcing are negligible, we obtain the equilibrium between the helicity injection (or viscous helicity dissipation) and SGS dissipation of resolved helicity:

$$\eta = -2\langle\tau_{ij}\tilde{R}_{ij}\rangle \equiv \langle\Pi_H\rangle, \quad (10)$$

which is analogous to the energy balance equation used by Lilly [18]:

$$\epsilon = -\langle\tau_{ij}\tilde{S}_{ij}\rangle = \langle\Pi_E\rangle, \quad (11)$$

where $\Pi_E \equiv -\tau_{ij}\tilde{S}_{ij}$ is the SGS energy dissipation rate.

As is well-known [18], from the energy balance relation Eq. (11), one obtains the Smagorinsky coefficient $c_s = \lambda_1^{-1/2}\left(\frac{3}{2}c_K\right)^{-3/4}/\pi$ (a cutoff filter is implied throughout this paper), where

$$\lambda_1 \equiv \frac{\langle(\tilde{S}_{ij}\tilde{S}_{ij})^{3/2}\rangle}{\langle\tilde{S}_{ij}\tilde{S}_{ij}\rangle^{3/2}} \quad (12)$$

is a moment correction factor, which is approximately a constant of order one in the inertial range. Now, given helicity balance relation Eq. (10), one can apply it to investigate the SGS helicity dissipation rate produced by the Smagorinsky model. Replacing the SGS stress in Eq. (10) with Smagorinsky model $\tau_{ij}=-2c_s^2\Delta^2|\tilde{S}|\tilde{S}_{ij}$, where $|\tilde{S}|\equiv(2\tilde{S}_{ij}\tilde{S}_{ij})^{1/2}$, we obtain

$$\eta = 4\sqrt{2}c_s^2\Delta^2\langle(\tilde{S}_{mn}\tilde{S}_{mn})^{1/2}\tilde{S}_{ij}\tilde{R}_{ij}\rangle. \quad (13)$$

Introducing another moment correction factor

$$\lambda_2 \equiv \frac{\langle (\tilde{S}_{ij}\tilde{S}_{ij})^{1/2}\tilde{S}_{mn}\tilde{R}_{mn}\rangle}{\langle \tilde{S}_{ij}\tilde{S}_{ij}\rangle^{1/2}\langle \tilde{S}_{mn}\tilde{R}_{mn}\rangle}, \tag{14}$$

the above equation can be written as

$$\eta = 4\sqrt{2}c_s^2\Delta^2\lambda_2\langle \tilde{S}_{ij}\tilde{S}_{ij}\rangle^{1/2}\langle \tilde{S}_{mn}\tilde{R}_{mn}\rangle. \tag{15}$$

Evaluating the second order moments by integrating the spectral tensor [Eq. (6)], we find after some algebra the expression for c_s, denoted c_s^H here, to be

$$c_s^H = \left[\frac{3}{4}\sqrt{6}\lambda_2 c_H c_K^{1/2}\pi^2\right]^{-1/2}. \tag{16}$$

c_s^H depends on c_H as well as c_K, while c_s depends only on c_K. Evaluating the expressions by putting $\lambda_1=\lambda_2=1$, $c_H=1.0$ and $c_K=1.6$ yields $c_s\approx 0.17$ while $c_s^H\approx 0.21$. Therefore we reach the important conclusion that the traditional Smagorinsky model underestimates the ensemble averaged helicity dissipation rate by a factor of $(0.17/0.21)^2\sim 0.63$. The Smagorinsky model is thus unable to correctly dissipate both energy and helicity simultaneously, assuming the "correct" statistics of $\tilde{S}_{ij}$ and $\tilde{R}_{ij}$ as implied by the spectra equations (6)–(8). One could then expect that when the Smagorinsky model is applied to the LES of helical turbulence with $c_s=0.17$, either the helicity is not dissipated enough or the resolved velocity field adjusts the $\tilde{S}_{ij}$ and $\tilde{R}_{ij}$ statistics away from what is implied from Eqs. (6)–(8), or both. Given the importance of the distribution of helicity in many helical flows as discussed previously, it is desirable to design a model that can dissipate both kinetic energy and helicity correctly, at least on average.

Note that the above conclusion does not change when we replace λ_1 and λ_2 with DNS values, since they are nearly equal in the inertial range. As will be shown later, in the inertial range $\lambda_1\approx 1.23$ while $\lambda_2\approx 1.25$, so that if these values are used we get $c_s\approx 0.15$ and $c_s^H\approx 0.19$, but the ratio is nearly unchanged.

It can also be seen that the value of c_H directly affects that of c_s^H, so the value of c_H will be confirmed again with DNS data later.

B. Helical SGS models

In view of the definition of the SGS helicity dissipation rate [see Eq. (4)], one has to control the correlation between the model for τ_{ij} and $\tilde{R}_{ij}$ in order to specify the SGS helicity dissipation rate. Therefore a two-term helical SGS model is proposed in the following form:

$$\tau_{ij} = -2C_1\Delta^2|\tilde{S}|\tilde{S}_{ij} - C_2\Delta^3|\tilde{S}|\tilde{R}_{ij}. \tag{17}$$

The two balance conditions between injection and SGS dissipation of resolved energy and helicity are used to determine the two model coefficients. The same idea has previously been applied to the joint balance of energy and enstrophy [23] and of energy and mean SGS stress [24]. Substituting the expression of τ_{ij} [Eq. (17)] into Eqs. (11) and (10), one can write

$$\epsilon = 2C_1\Delta^2\langle|\tilde{S}|\tilde{S}_{ij}\tilde{S}_{ij}\rangle + C_2\Delta^3\langle|\tilde{S}|\tilde{R}_{ij}\tilde{S}_{ij}\rangle, \tag{18}$$

$$\eta = 4C_1\Delta^2\langle|\tilde{S}|\tilde{S}_{ij}\tilde{R}_{ij}\rangle + 2C_2\Delta^3\langle|\tilde{S}|\tilde{R}_{ij}\tilde{R}_{ij}\rangle. \tag{19}$$

Defining another moment correction factor

$$\lambda_3 \equiv \frac{\langle (\tilde{S}_{mn}\tilde{S}_{mn})^{1/2}\tilde{R}_{ij}\tilde{R}_{ij}\rangle}{\langle \tilde{S}_{mn}\tilde{S}_{mn}\rangle^{1/2}\langle \tilde{R}_{ij}\tilde{R}_{ij}\rangle}, \tag{20}$$

the correlations in the equations can be expressed in terms of second order ones and thus can be evaluated by integrating the spectral energy density tensor. After some algebra, the equations are simplified to

$$1 = \left[\frac{3\sqrt{6}}{4}\lambda_1 c_K^{3/2}\pi^2\right]C_1 + \left[\frac{3\sqrt{6}}{16}\lambda_2 c_K^{1/2}c_H\pi^2\right]\eta^* C_2,$$

$$\eta^* = \left[\frac{3\sqrt{6}}{4}\lambda_2 c_K^{1/2}c_H\pi^2\right]\eta^* C_1 + \left[\frac{3\sqrt{6}}{10}\lambda_3 c_K^{3/2}\pi^4\right]C_2, \tag{21}$$

in which $\eta^* \equiv \eta\Delta/\epsilon$ is the nondimensional helicity injection rate. Solving the equations gives C_1 and C_2 as functions of η^*:

$$C_1 = \frac{\left[\left(\frac{3}{2}c_K\right)^{3/2}\lambda_1\pi^2\right]^{-1}\left[1 - \frac{5}{8}\lambda_2\lambda_3^{-1}c_K^{-1}c_H\pi^{-2}\eta^{*2}\right]}{1 - \frac{5}{8}\lambda_2^2\lambda_1^{-1}\lambda_3^{-1}c_H^2c_K^{-2}\pi^{-2}\eta^{*2}}, \tag{22}$$

$$C_2 = \frac{[5\sqrt{6}(\lambda_1 c_K - \lambda_2 c_H)]\eta^*}{9\lambda_1\lambda_3 c_K^{5/2}\pi^4\left[1 - \frac{5}{8}\lambda_2^2\lambda_1^{-1}\lambda_3^{-1}c_H^2c_K^{-2}\pi^{-2}\eta^{*2}\right]}. \tag{23}$$

Notice that since $\tilde{R}_{ij}$ is a pseudotensor and, as an odd function of the pseudoscalar η^*, C_2 is also a pseudoscalar, the second term in the model expression Eq. (17) as a whole is a true tensor, having the same parity symmetry as the real SGS stress. For the particular case of nonhelical turbulence where $\eta^*=0$, C_2 becomes zero while C_1 reduces consistently to the expression obtained from energy dissipation balance, so that the traditional Smagorinsky model is recovered.

To clearly see the dependence of C_1 and C_2 on η^*, Eqs. (22) and (23) are plotted in Fig. 1, with $c_K=1.6$, $c_H=1.0$, and the λ's are all set to be one. Also plotted are linear approximations, obtained as Taylor-series expansions around $\eta^*=0$:

$$C_1 = [(3c_K/2)^{3/2}\lambda_1\pi^2]^{-1} \approx 0.027, \tag{24}$$

$$C_2 = \frac{5\sqrt{6}(\lambda_1 c_K - \lambda_2 c_H)}{9\lambda_1\lambda_3 c_K^{5/2}\pi^4}\eta^* \approx 0.0026\eta^*. \tag{25}$$

We can see that the magnitude of C_1 decreases with increasing $|\eta^*|$ while C_2 increases with η^*, but the dependence on η^* does not depart much away from the linear approximation in the neighborhood of the origin. Recalling that the helicity and energy injection rates are related by the inequality $|\eta| \leq 2k_f\epsilon$ for positive energy injection rate, where k_f is the maximal forcing wave number, one can estimate $|\eta^*|$

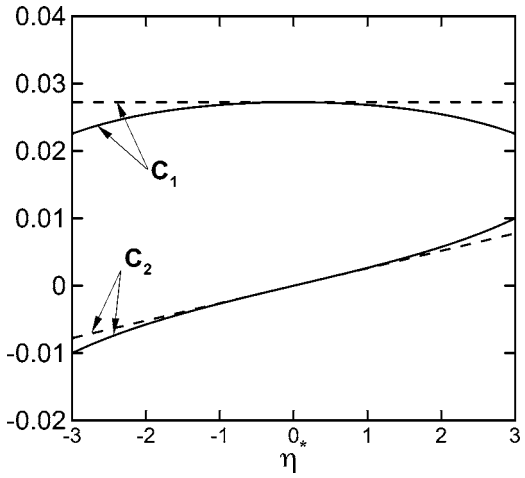

FIG. 1. C_1 and C_2 and their linearization as functions of η^*. Solid lines: complete formulas [Eqs. (22) and (23)]; and dashed lines: linearization [Eqs. (24) and (25)].

$\leqslant 2k_f\Delta \sim 2\pi\Delta/l$ for the common cases in which the helicity is injected at the integral scale l of the flow field. Therefore, consistent with the assumptions already made, Δ/l and thus η^* are presumably much smaller than one, so that one can safely replace the coefficients with the linear approximations.

With the linearized coefficients, the energy balance equation is then not satisfied exactly. Substituting C_1 and C_2 in the rhs of the first equation in Eq. (21) with the linearized solutions Eqs. (24) and (25), the rhs of the equation becomes

$$1 + \frac{5\lambda_2 c_H(\lambda_1 c_K - \lambda_2 c_H)}{8\lambda_1\lambda_3\pi^2 c_K^2}\eta^{*2} \approx 1 + 0.01\,\eta^{*2}. \tag{26}$$

Therefore the relative error in satisfying the energy balance is about $0.01\eta^{*2}$, which for small η^* is negligible. On the other hand, substitution of C_1 and C_2 in the rhs of the second equation in Eq. (21) with the linearized coefficients shows that the helicity balance equation is satisfied exactly. Thus the linearization does not introduce error in the helicity balance equation.

The model obtained as such is a nonlocal one, in the sense that C_2 depends on η^*, which is an ensemble averaged quantity and cannot be calculated from the local flow field. Thus in its present form the model cannot be applied in cases in which the mean helicity and energy injection rates are not known *a priori*.

In order to obtain a model that is useable in practice, η^* has to be evaluated with some quantity that can be calculated locally. After several trials, we choose to model η^* as $\tilde{S}_{ij}\tilde{R}_{ij}/(|\tilde{S}||\tilde{R}|)$, in which $|\tilde{R}| \equiv (2\tilde{R}_{ij}\tilde{R}_{ij})^{1/2}$. The first advantage of this expression is that, thanks to Schwartz inequality, it shares the same boundedness property with η^*. As a consequence, it has improved chances of robustness in numerical simulation. Second, the helicity dissipation rate is defined as $\eta \equiv 4\nu\langle S'_{ij}R'_{ij}\rangle$. By replacing the two tensors in this definition with corresponding filtered ones, the model expression loses the correspondence in magnitude, but arguably some of the geometric properties (for example, the relative orientation between the tensors) are partially retained. Finally this expression is simple, so that it is possible to determine the coefficients of the model by the same method applied above. Another estimation for η^* that was explored is as follows:

$$\eta = -2\langle\tau_{ij}\tilde{R}_{ij}\rangle \sim -2\langle L_{ij}\tilde{R}_{ij}\rangle \sim -L_{ij}\tilde{R}_{ij}, \tag{27}$$

and $\epsilon \sim -L_{ij}\tilde{S}_{ij}$, where $L_{ij} \equiv \widetilde{\tilde{u}_i\tilde{u}_j} - \tilde{\tilde{u}}_i\tilde{\tilde{u}}_j$ is the Leonard stress, so that

$$\eta^* \sim \frac{\Delta L_{ij}\tilde{R}_{ij}}{L_{mn}\tilde{S}_{mn}}. \tag{28}$$

While this estimate falls closer to the energy and helicity dissipation, it does not possess the above-mentioned desirable properties (e.g., it is unbounded since the denominator can vanish) and is thus not pursued further.

Replacing the η^* in the expression for C_2 [Eq. (25)] with the model expression, one arrives at a local formulation for the helical model

$$\tau_{ij} = -2C_1\Delta^2|\tilde{S}|\tilde{S}_{ij} - \beta\Delta^3\frac{\tilde{R}_{mn}\tilde{S}_{mn}}{|\tilde{R}|}\tilde{R}_{ij}, \tag{29}$$

in which C_1 and β are model coefficients. Since the model formulation has been changed, the coefficients have to be adjusted to satisfy the energy and helicity dissipation balance conditions. The coefficients can be found by repeating the previous calculation for the nonlocal model. For the sake of completeness, we list the resulting energy and helicity balance relations:

$$\epsilon = 2C_1\Delta^2\langle|\tilde{S}|\tilde{S}_{ij}\tilde{S}_{ij}\rangle + \beta\Delta^3\langle|\tilde{R}|^{-1}(\tilde{R}_{ij}\tilde{S}_{ij})^2\rangle, \tag{30}$$

$$\eta = 4C_1\Delta^2\langle|\tilde{S}|\tilde{S}_{ij}\tilde{R}_{ij}\rangle + 2\beta\Delta^3\langle|\tilde{R}|^{-1}\tilde{R}_{mn}\tilde{S}_{mn}\tilde{R}_{ij}\tilde{R}_{ij}\rangle, \tag{31}$$

and the simplified dimensionless versions obtained from Kolmogorov spectra:

$$\begin{aligned} 1 &= \left[\frac{3\sqrt{6}}{4}\lambda_1\pi^2 c_K^{3/2}\right]C_1 + \left[\frac{3\sqrt{15}}{64}\lambda_4\pi c_K^{-1/2}c_H^2\right]\eta^{*2}\beta, \\ 1 &= \left[\frac{3\sqrt{6}}{4}\lambda_2\pi^2 c_K^{1/2}c_H\right]C_1 + \left[\frac{3\sqrt{15}}{40}\lambda_5\pi^3 c_K^{1/2}c_H\right]\beta, \end{aligned} \tag{32}$$

in which

$$\lambda_4 \equiv \frac{\langle(\tilde{R}_{ij}\tilde{S}_{ij})^2(\tilde{R}_{mn}\tilde{R}_{mn})^{-1/2}\rangle}{\langle\tilde{R}_{ij}\tilde{S}_{ij}\rangle^2\langle\tilde{R}_{mn}\tilde{R}_{mn}\rangle^{-1/2}}, \tag{33}$$

$$\lambda_5 \equiv \frac{\langle(\tilde{R}_{ij}\tilde{S}_{ij})(\tilde{R}_{mn}\tilde{R}_{mn})^{1/2}\rangle}{\langle\tilde{R}_{ij}\tilde{S}_{ij}\rangle\langle\tilde{R}_{mn}\tilde{R}_{mn}\rangle^{1/2}}. \tag{34}$$

From the above equations, C_1 and β are found to be

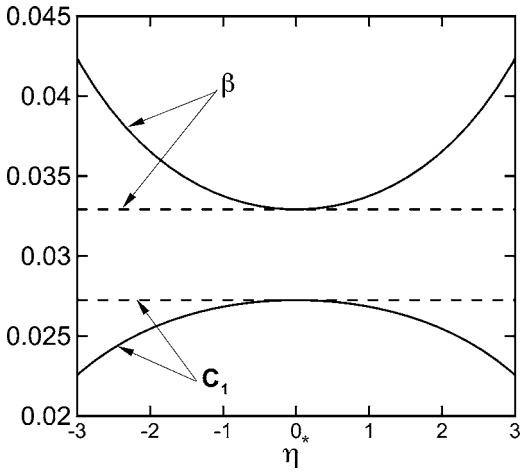

FIG. 2. C_1 and β and their linearization as functions of η^*. Solid lines: complete formulas [Eqs. (35) and (36)], and dashed lines: linearization [Eqs. (37) and (38)].

$$C_1 = \frac{\left[\left(\frac{3}{2}c_K\right)^{3/2}\pi^2\lambda_1\right]^{-1}\left[1-\frac{5}{8}\lambda_4\lambda_5^{-1}\pi^{-2}c_H c_K^{-1}\eta^{*2}\right]}{1-\frac{5}{8}\lambda_2\lambda_4\lambda_1^{-1}\lambda_5^{-1}\pi^{-2}c_K^{-2}c_H^2\eta^{*2}}, \tag{35}$$

$$\beta = \frac{8\sqrt{15}(\lambda_1 c_K - \lambda_2 c_H)\pi^{-3}\lambda_1^{-1}\lambda_5^{-1}c_K^{-3/2}c_H^{-1}}{9\left[1-\frac{5}{8}\lambda_2\lambda_4\lambda_1^{-1}\lambda_5^{-1}\pi^{-2}c_K^{-2}c_H^2\eta^{*2}\right]}. \tag{36}$$

The linear approximations of C_1 and β are easily seen to be constants

$$C_1 = [(3c_K/2)^{3/2}\pi^2\lambda_1]^{-1}, \tag{37}$$

$$\beta = \frac{8}{9}\sqrt{15}(\lambda_1 c_K - \lambda_2 c_H)\pi^{-3}\lambda_1^{-1}\lambda_5^{-1}c_K^{-3/2}c_H^{-1}, \tag{38}$$

which assume the values

$$C_1 = 0.027, \quad \beta = 0.033 \tag{39}$$

if all the λ's are set to one and $c_K=1.6$ and $c_H=1.0$.

The coefficients, along with the linear approximations, are plotted in Fig. 2 as functions of η^*. As before, we can use the linear approximation as the model coefficients, and thus obtain a local model whose coefficients are constants. As in the case of the nonlocal model, the helicity balance equation is exactly satisfied by the linearized coefficients, which can be shown by simple substitution. On the other hand, the error in satisfying energy balance can not be analytically determined because DNS data shows that λ_4 varies much more than the other correction factors in the inertial range, therefore the estimation assuming $\lambda_4=1$ does not give the correct answer. Note that λ_4 does not affect the values of the linearized coefficients, although it affects the range in which the linear approximation is accurate. Later we will check the accuracy of the linear approximation by analyzing the DNS data.

C. Dynamic models

In most applications, calculating the model coefficients by the dynamic procedure [19] and its variants has improved the model performance. Therefore, in this section, the dynamic versions of the nonlocal helical model are derived.

We start from the Germano identity [19]:

$$L_{ij} = T_{ij} - \hat{\tau}_{ij} \tag{40}$$

where the wide hat denotes test-filtering; T_{ij} is the SGS stress defined at test filter scale, and L_{ij} is the Leonard stress: $L_{ij} \equiv \widehat{\tilde{u}_i\tilde{u}_j} - \hat{\tilde{u}}_i\hat{\tilde{u}}_j$. τ_{ij} is modeled by Eq. (17). The same applies to T_{ij}, only with the filter being replaced by the test filter. In this section $\tilde{\Delta}$ (instead of Δ) denotes the filter size, while the scale of test filter is denoted as $\hat{\tilde{\Delta}}$:

$$T_{ij} = -2C_1\hat{\tilde{\Delta}}^2|\hat{\tilde{S}}|\hat{\tilde{S}}_{ij} - C_2\hat{\tilde{\Delta}}^3|\hat{\tilde{S}}|\hat{\tilde{R}}_{ij}. \tag{41}$$

Therefore we have assumed that the coefficients are scale-invariant [25]. Substituting τ_{ij} and T_{ij} into the Germano identity, we obtain

$$L_{ij} = C_1 M_{ij} + C_2 P_{ij}, \tag{42}$$

where

$$M_{ij} = 2\tilde{\Delta}^2\widehat{|\tilde{S}|\tilde{S}_{ij}} - 2\hat{\tilde{\Delta}}^2|\hat{\tilde{S}}|\hat{\tilde{S}}_{ij}, \tag{43}$$

$$P_{ij} = \tilde{\Delta}^3\widehat{|\tilde{S}|\tilde{R}_{ij}} - \hat{\tilde{\Delta}}^3|\hat{\tilde{S}}|\hat{\tilde{R}}_{ij}. \tag{44}$$

By minimizing the mean-squared error $\langle(L_{ij}-C_1M_{ij}-C_2P_{ij})^2\rangle_v$ in satisfying Eq. (42), where $\langle\cdot\rangle_v$ denotes volume-averaging over the whole flow field, the coefficients are found to be

$$C_1 = \frac{\langle L_{ij}M_{ij}\rangle_v\langle P_{lk}P_{lk}\rangle_v - \langle L_{ij}P_{ij}\rangle_v\langle P_{lk}M_{lk}\rangle_v}{\langle M_{ij}M_{ij}\rangle_v\langle P_{lk}P_{lk}\rangle_v - \langle P_{ij}M_{ij}\rangle_v^2}, \tag{45}$$

$$C_2 = \frac{\langle L_{ij}P_{ij}\rangle_v\langle M_{lk}M_{lk}\rangle_v - \langle L_{ij}M_{ij}\rangle_v\langle P_{lk}M_{lk}\rangle_v}{\langle M_{ij}M_{ij}\rangle_v\langle P_{lk}P_{lk}\rangle_v - \langle P_{ij}M_{ij}\rangle_v^2}. \tag{46}$$

As mentioned in Sec. I, flows characterized with strong helicity are often found in the large-scale structure of the atmosphere, in which the Coriolis force also plays an important role. Therefore it is often of interest to formulate the model in a rotating frame. In the modeling of rotating turbulence, the property of material frame difference or indifference should be taken into account [26]. As was already established in the literature, the SGS stress is not material frame indifferent. Specifically, the stress τ_{ij} in an inertial frame and that in a rotating frame τ_{ij}^r are related by [27]

$$Q_{il}Q_{jk}\tau_{lk} = \tau_{ij}^r + Z_{ij}^r, \tag{47}$$

in which the superscript r denotes quantities in the rotating frame; Q_{ij} is a time-dependent rotation matrix transforming the coordinates in the inertial frame into the rotating frame; and Z_{ij}^r is given as [27]

$$Z_{ij}^r = \varepsilon_{ilk}\Omega_l^r(\widetilde{x_k^r u_j^r} - x_k^r \tilde{u}_j^r) + \varepsilon_{jmn}\Omega_m^r(\widetilde{x_n^r u_i^r} - x_n^r \tilde{u}_i^r) + \varepsilon_{ilk}\varepsilon_{jmn}\Omega_l^r\Omega_m^r(\widetilde{x_k^r x_n^r} - x_k^r x_n^r). \quad (48)$$

Similarly the Leonard stress is also material frame different. However, the usual models including the Smagorinsky model and the present helical model [Eq. (17)] are material frame indifferent. Therefore if we insist that the Germano identity applied in the rotating frame should be derived from the inertial frame by the time-dependent rotation, the material frame indifferent models should satisfy

$$L_{ij}^r + Z_{ij}^{rt} = T_{ij}^r - \hat{\tau}_{ij}^r, \quad (49)$$

where Z_{ij}^{rt} is defined in the same way as Z_{ij}^r but for resolved velocity field and with the filter replaced by the test filter. The presence of Z_{ij}^{rt} will lead to unphysical oscillation in the dynamically determined coefficients [28] in some cases. One way to remedy this problem is to develop model expressions that observe the same rules of transformation as the true SGS stress as given by Eq. (47) so that the same form of the Germano identity is satisfied in both the inertial and rotating frame by the models; but, based on the present material frame indifferent model expressions, we can also circumvent the problem by applying the Germano identity in the form of SGS force:

$$\partial_j L_{ij} = \partial_j T_{ij} - \partial_j \hat{\tau}_{ij}. \quad (50)$$

Given that Z_{ij}^{rt} is divergence-free for a spherically symmetric filter [27], Eq. (50) is material frame indifferent and therefore it is directly applicable in a rotating frame. The dynamic coefficients derived from Eq. (50) will be material frame indifferent and are expected to be well-behaved in different frames of reference.

We now calculate the coefficients for the nonlocal model by using Eq. (50). Following the same procedure it is easy to find that

$$C_1 = \frac{\langle P_i P_i\rangle_v \langle M_j \partial_k L_{jk}\rangle_v - \langle P_i M_i\rangle_v \langle P_j \partial_k L_{jk}\rangle_v}{\langle P_i P_i\rangle_v \langle M_j M_j\rangle_v - \langle P_i M_i\rangle_v^2}, \quad (51)$$

$$C_2 = \frac{\langle M_i M_i\rangle_v \langle P_j \partial_k L_{jk}\rangle_v - \langle P_i M_i\rangle_v \langle M_j \partial_k L_{jk}\rangle_v}{\langle P_i P_i\rangle_v \langle M_j M_j\rangle_v - \langle P_i M_i\rangle_v^2}, \quad (52)$$

where

$$M_i = 2\tilde{\Delta}^2 \partial_j(\widetilde{|\tilde{S}|\tilde{S}_{ij}}) - \hat{\tilde{\Delta}}^2 \partial_j(|\hat{\tilde{S}}|\hat{\tilde{S}}_{ij}), \quad (53)$$

$$P_i = \tilde{\Delta}^3 \partial_j(\widetilde{|\tilde{S}|\tilde{R}_{ij}}) - \hat{\tilde{\Delta}}^3 \partial_j(|\hat{\tilde{S}}|\hat{\tilde{R}}_{ij}). \quad (54)$$

In what follows, the first dynamic model [Eqs. (45) and (46)] is called Dyn-A while the second one [Eqs. (51) and (52)] is called Dyn-B. The test filter $\hat{\tilde{\Delta}}$ is taken to be $2\tilde{\Delta} \equiv 2\Delta$.

III. NUMERICAL TESTS OF THE HELICAL MODELS

A. *A priori* tests in isotropic turbulence

In this section, the model performance and the assumptions involved in the above analysis are validated *a priori*. The data are obtained from a 512^3 DNS of an isotropic steady turbulent flow with constant energy and helicity injection rate, $\epsilon=0.1$ and $\eta=0.5$, respectively. The Taylor-scale Reynolds number is about 220.

Figure 3 shows the energy and helicity spectra calculated from the DNS data set and the ones predicted from Kolmogorov phenomenology [Eqs. (7) and (8)] with $c_K=1.6$ and $c_H=1.0$. For this resolution, the spectra display only narrow inertial ranges. The helicity spectrum shows that the coefficient c_H seems to be around 1.0, confirming the value found previously in the DNS of the NS equation with hyperviscosity [4].

Figure 4 shows the dependence of $\lambda_1-\lambda_5$ on filter scale Δ.

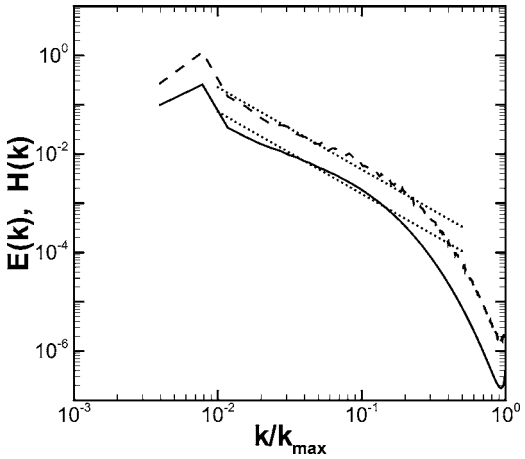

FIG. 3. Energy and helicity spectra. Solid line: energy spectrum; dashed line: helicity spectrum; and dotted line: $-5/3$ law. Lower dotted line: $c_K\epsilon^{2/3}k^{-5/3}$ with $c_K=1.6$ and $\epsilon=0.1$; and upper dotted line: $c_H\eta\epsilon^{-1/3}k^{-5/3}$ with $c_H=1.0$, $\epsilon=0.1$, and $\eta=0.5$.

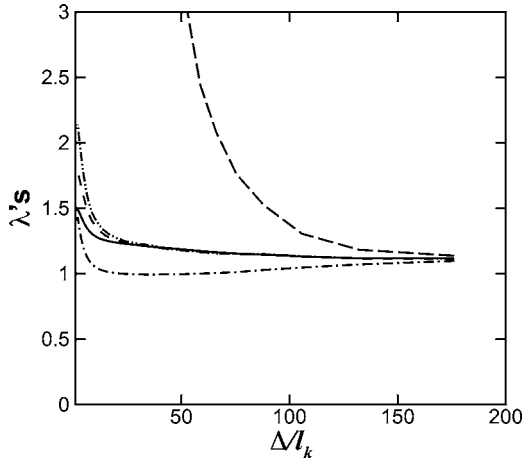

FIG. 4. Dependence of the λ's on filter size Δ. The line patterns from λ_1 to λ_5 are, respectively, solid line, dashed, dotted, long dashed, and dash-dot-dotted. $l_k \equiv (\nu^3/\epsilon)^{1/4}$ is the Kolmogorov length scale.

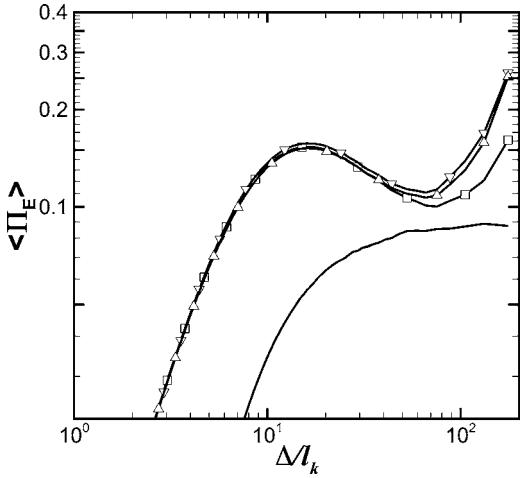

FIG. 5. The dependence of SGS energy dissipation rate on filter size. Solid line: DNS data, line with squares: the Smagorinsky model, line with deltas: the nonlocal helical model, and line with gradients: the local helical model. $l_k \equiv (\nu^3/\epsilon)^{1/4}$ is the Kolmogorov length scale.

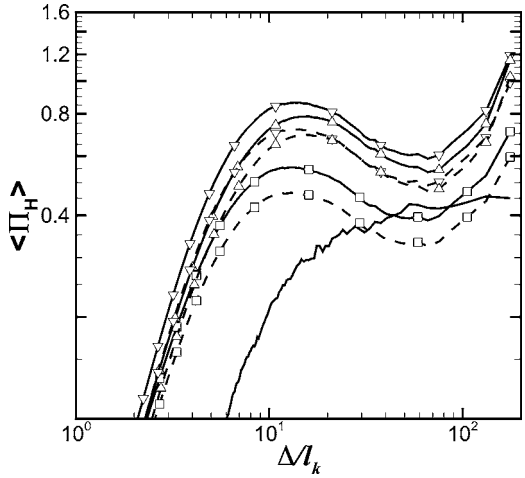

FIG. 6. The dependence of SGS helicity dissipation rate on filter size. Solid line: DNS data, line with squares: the Smagorinsky model, line with deltas: the nonlocal helical model, and line with gradients: the local helical model. The solid lines correspond to models with coefficients calculated by assuming the λ's are one, while the dashed line corresponds to DNS λ's. $l_k \equiv (\nu^3/\epsilon)^{1/4}$ is the Kolmogorov length scale.

Except λ_4, all the other four coefficients are almost constant and close to one in the inertial range, although the values increase when the filter size approaches the Kolmogorov scale. The constant values for the coefficients are, respectively, $\lambda_1 \approx 1.19$, $\lambda_2 \approx 1.20$, $\lambda_3 \approx 1.01$, and $\lambda_5 \approx 1.20$ (averaged from $\Delta/l_k \sim 20$ to around 170). On the other hand, λ_4 depends quite strongly on the filter size, although it too appears to tend to values $O(1)$ for $\Delta/l_k \gg 1$. As mentioned before, this trend renders it difficult to estimate analytically the relative error introduced by the linearization into the SGS energy dissipation calculated from the local model. Next we will check the error numerically by calculating the SGS energy dissipation produced by the models from DNS data.

The mean SGS energy dissipation $\langle \Pi_E \rangle$ and helicity dissipation $\langle \Pi_H \rangle$ calculated *a priori* from the Smagorinsky model and the pair of helical models are compared with DNS data for different filter scale in Figs. 5 and 6. Note that the present model derivations are valid only in the inertial range. It is well-known that in the viscous range molecular dissipation affects the model coefficients, but this has not been included in our analysis. As a consequence, the model dissipations are significantly overpredicted in the viscous range at $\Delta/l_k < 50$. For more discussions on the transition to the viscous range, see [29]. Moreover, since we have set $\lambda_1 = 1$ in determining the theoretical value of the coefficients (whereas the real value of λ_1 may be 10%–20% higher, see Fig. 4), the model dissipation using the theoretical coefficient value is expected to be overpredicted even in the inertial range. Indeed the Smagorinsky model overestimates the SGS energy dissipation by about 20%, as is clear from Fig. 5. On the other hand, the SGS energy dissipation rates predicted by the helical models are only higher than that of Smagorinsky in the inertial range by small amounts. This overestimate is for the most part caused by the error in the model coefficients introduced by the linearization. As has already been proven analytically, the overestimate by the nonlocal model due to the linearization is approximately $0.01\eta^{*2}$, and thus decreases with filter size Δ for fixed ϵ and η. This trend is consistently observed in Fig. 5. The prediction of the local helical model is about 20% higher than that of the Smagorinsky model in the lower end of the inertial range, and the relative error decreases with the filter size, however, with a rate slower than for the nonlocal model. Therefore the relative error in the SGS energy dissipation calculated *a priori* by the local helical model is at an acceptable level, and shows simple dependence on the filter size. Assuming $\lambda_4 = 1$ does not have significant adverse effect, even though λ_4 shows relative strong dependence on filter size. The increase of $\langle \Pi_E \rangle$ predicted by the models seen at large filter scales $(\Delta/l_k > 100)$ is due to the effects of the forcing term which directly increases the variances of $\tilde{S}_{ij}$ and $\tilde{R}_{ij}$ at those scales. As will be seen in Fig. 6, a similar increase in $\langle \Pi_H \rangle$ predicted from the models is also observed for the same reason.

Figure 6 shows the SGS helicity dissipation rates predicted by the various models. In order to quantitatively verify the theoretical result, we calculate the SGS helicity dissipation rates predicted by the models with DNS values of the λ's, which are plotted with dashed lines in Fig. 6. It can be seen in the figure that the SGS helicity dissipation rate calculated from the Smagorinsky model is lower than the DNS value by about 30%, close to the theoretical result. It confirms that the Smagorinsky model is unable to correctly predict the SGS helicity and energy dissipation simultaneously. The SGS helicity dissipation predicted by the helical models is closer, and reaches a value of about 0.5 in the higher wave-number end of the inertial range. Notice that when the Re number tends to infinity, the level of SGS helicity dissipation rate should approach the helicity injection rate $\eta = 0.5$, while, due to the finite Re number effect in the data, the SGS helicity dissipation calculated from the DNS data is only about 0.45 in the inertial range. Taking these effects into account, the error introduced by replacing the

model coefficients with their linearization appears to be rather small in the inertial range.

B. *A posteriori* tests in isotropic turbulence

In this section, the helical models are applied to the LES of isotropic steady and decaying turbulence and the results are compared with DNS data obtained through additional simulations. Also tested are the dynamic Smagorinsky model and the dynamic mixed nonlinear model (for specific definitions used in this latter model, see [30]). In the simulations, the rotational form of the NS equation is solved by the pseudospectral method in Fourier space in a $[0,2\pi]^3$ box. The resolution of LES is 64^3. The reference DNS is done with resolution 256^3 for forced turbulence and 512^3 for decaying turbulence.

1. Isotropic steady turbulence

For the simulation of steady forced turbulence, the velocity field is initialized with Gaussian random numbers and is then rescaled to match a prescribed (initial) energy spectrum in the form of $E_0(k)=A(u_0^2/k_p)(k/k_p)^4\exp(-2k^2/k_p^2)$ where k_p and A are constants, k_p characterizes the initial integral length scale and A is chosen in such a way that the initial turbulent kinetic energy is $3u_0^2/2$. A statistically steady state is achieved by injecting constant amounts of helicity and energy into the flow field by the forcing term in the NS equation. The force is given in Fourier space in the following form:

$$\hat{\boldsymbol{f}}(\mathbf{k},t)=f_u(t)\hat{\boldsymbol{u}}(\mathbf{k},t)+f_o(t)\hat{\boldsymbol{\omega}}(\mathbf{k},t), \tag{55}$$

in which f_u and f_o are updated at each time step to keep the energy and helicity injection rate ϵ and η constant. From the definition of ϵ and η:

$$\epsilon=\langle f_i u_i\rangle=\sum\langle\hat{f}_i(\mathbf{k},t)\hat{u}_i^*(\mathbf{k},t)\rangle, \tag{56}$$

$$\eta=2\langle f_i\omega_i\rangle=2\sum\langle\hat{f}_i(\mathbf{k},t)\hat{\omega}_i^*(\mathbf{k},t)\rangle, \tag{57}$$

we obtain two algebraic equations for f_u and f_o, from which they are solved to be

$$f_u=\frac{\epsilon\sum\langle\hat{\omega}_i\hat{\omega}_i^*\rangle-\frac{1}{2}\eta\sum\langle\hat{\omega}_i\hat{u}_i^*\rangle}{\sum\langle\hat{u}_i\hat{u}_i^*\rangle\sum\langle\hat{\omega}_i\hat{\omega}_i^*\rangle-\left[\sum\langle\hat{\omega}_i\hat{u}_i^*\rangle\right]^2}, \tag{58}$$

$$f_o=\frac{\frac{1}{2}\eta\sum\langle\hat{u}_i\hat{u}_i^*\rangle-\epsilon\sum\langle\hat{\omega}_i\hat{u}_i^*\rangle}{\sum\langle\hat{u}_i\hat{u}_i^*\rangle\sum\langle\hat{\omega}_i\hat{\omega}_i^*\rangle-\left[\sum\langle\hat{\omega}_i\hat{u}_i^*\rangle\right]^2}, \tag{59}$$

where the summation is over the sphere $|\mathbf{k}|<k_f\equiv 2$. In the simulations, $\epsilon=0.1$ and $\eta=0.3$, so the helicity injection rate is close to the maximal value $\eta_{\max}=2k_f\epsilon=0.4$ [31]. The results of LES are averaged over about four eddy turn-over time scales $\tau\equiv(2K)/(3\epsilon)\approx 3.333$ after the turbulence reaches steady state, where K is the mean kinetic energy in steady state, while those of DNS are averaged over about three eddy turn-over time scales. The Reynolds number for the DNS data is about 175.

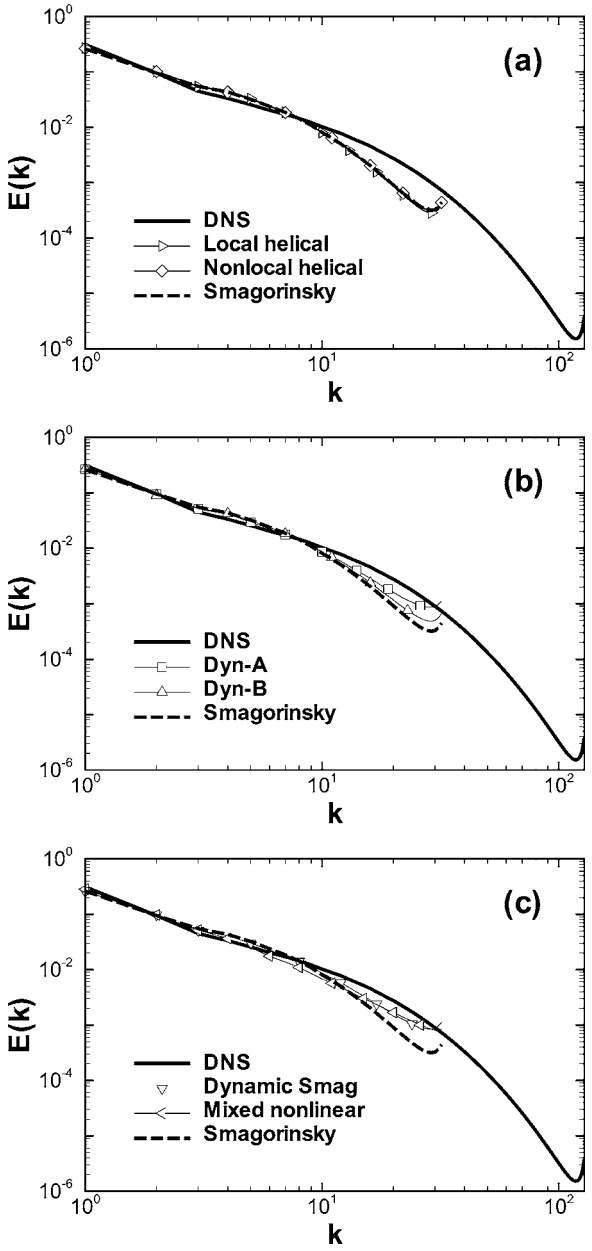

FIG. 7. Energy spectra. Solid line without symbol: DNS; dashed lines: Smagorinsky; and thin solid lines with symbols: the other models. In (a) local helical model (right triangles) and nonlocal helical (diamonds), (b) Dyn-A (squares) and Dyn-B (deltas), and (c) dynamic Smagorinsky (gradients) and mixed nonlinear (left triangles).

Figure 7 shows the energy spectra calculated by the different models. As designed, the effect of the added helical term in the local and nonlocal helical models on the energy spectrum is negligible. Only small differences are observed among the models, mainly at the high wave-number end. The dynamic models display the widely observed trend in nonhelical turbulence, that is, compared with nondynamic models, they predict higher spectral level near the cutoff wave number and lower level at the middle range of wave number. The

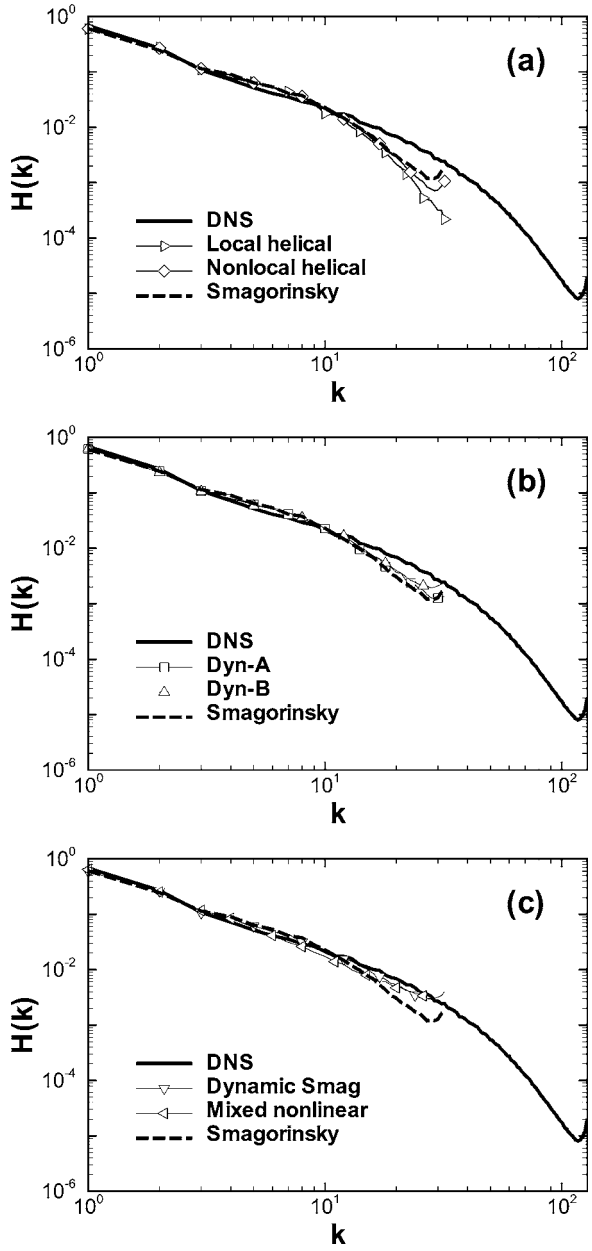

FIG. 8. Helicity spectra. Lines and symbols are the same as in Fig. 7.

Dyn-B model is more dissipative than the Dyn-A model at the high wave-number region. The results for the dynamic Smagorinsky model and the dynamic mixed nonlinear model are the same as those observed in nonhelical turbulence [30].

Figure 8 shows the calculated helicity spectra. The spectrum calculated by the Smagorinsky model, as compared with the DNS result, shows a trend similar to the energy spectrum. All the models give close results at the middle part of the wave-number space. Near the cutoff scale, the dynamic Smagorinsky and dynamic mixed nonlinear model give the highest level and are closest to the DNS results. For the nonlocal, local helical models and Dyn-A model, the added helical term dissipates too much helicity, so that the spectra are lower than the DNS results. The spectrum calculated by the Dyn-B model falls in between the above two groups.

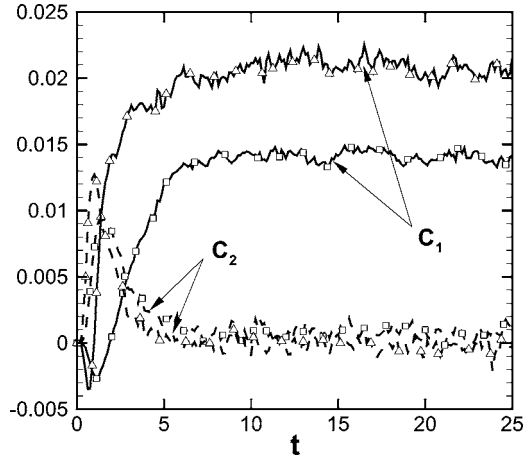

FIG. 9. Time evolution of the dynamically calculated coefficients. Square: Dyn-A model; and delta: Dyn-B model.

Shown in Fig. 9 are the dynamically calculated coefficients C_1 and C_2 for both the Dyn-A and Dyn-B models. Because the helical term is proportional to the highly intermittent quantity $\tilde{R}_{ij}$, the coefficients display relatively strong fluctuations around their means. Two observations about the Dyn-A model can be made. First, the dynamically calculated coefficient C_2 is only slightly higher that the value calculated from the Kolmogorov spectrum, which is about 0.0008 from Eq. (25) for $\epsilon=0.1$, $\eta=0.3$, and $\Delta=\pi/32$. Second, the value of C_1 is lower than the previously found value in the LES of high Re number flow [30], due to the effects of low Re number and the helical term. It can also be seen that the mean value of C_2 for the Dyn-B model is nearly zero, showing that the helical term in the Dyn-B model is negligible.

2. Decaying isotropic turbulence

For the simulation of decaying turbulence, the flow field has to be initialized with controlled helicity. One way to do this, as proposed in [13], is to manipulate the real and imaginary parts of the Fourier components of the velocity field. Here we propose another method based on the helical wave decomposition [22,31,32]. Assuming that $\boldsymbol{h}_+(\mathbf{k})$ and $\boldsymbol{h}_-(\mathbf{k})$ are, respectively, the amplitude of the normalized positive and negative helical waves, which constitute an orthonormal base in the plane perpendicular to the wave vector $\mathbf{k}$, the Fourier component of the initial velocity field is prescribed as

$$\hat{\boldsymbol{u}}(\mathbf{k}) = B[a_+\boldsymbol{h}_+(\mathbf{k}) + a_-\boldsymbol{h}_-(\mathbf{k})][E_0(k)/(4\pi k^2)]^{1/2}, \quad (60)$$

where $E_0(k)$ is defined in the previous section; a_+ and a_- are independent Gaussian random numbers; and B is a scaling parameter. The variance of a_+ is fixed to be one, i.e., $\langle|a_+|^2\rangle=1$, but that of a_- is determined by the magnitude of the helicity we want to put into the flow field. Notice that the helicity spectrum corresponding to the above velocity distribution is [31]

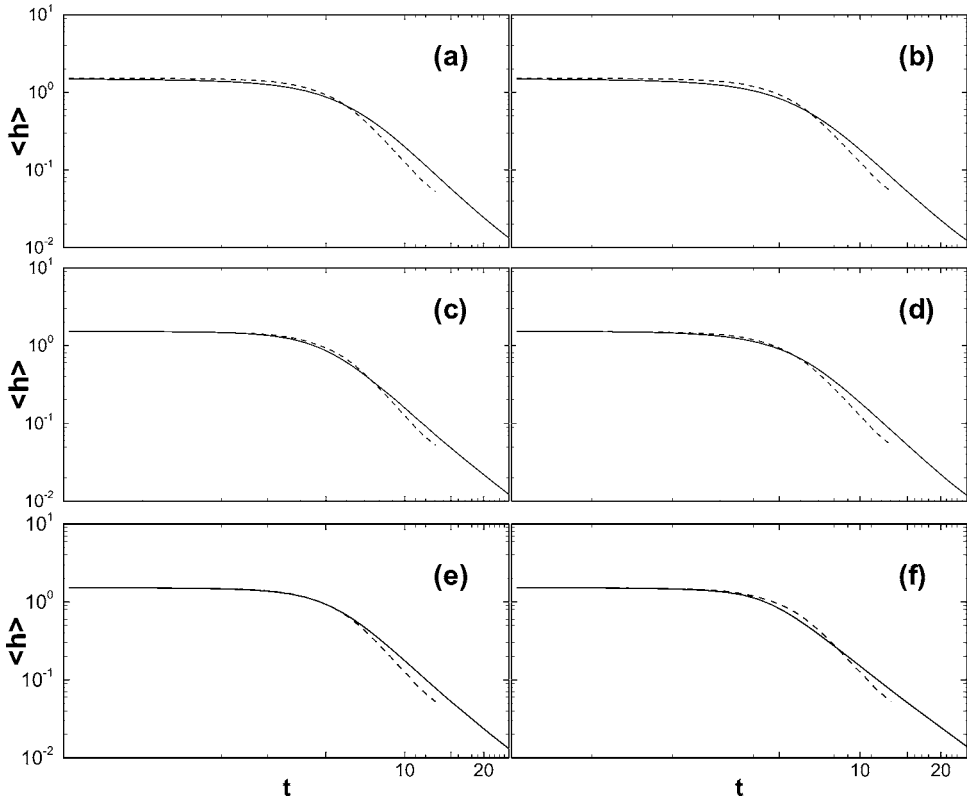

FIG. 10. The decay of mean helicity. Dashed line: DNS; and solid lines: models. (a) Smagorinsky; (b) local helical; (c) Dyn-A; (d) Dyn-B; (e) dynamic Smagorinsky; and (f) mixed nonlinear.

$$H(k) = kB^2(\langle|a_+|^2\rangle - \langle|a_-|^2\rangle)E_0(k)$$
$$= kB^2(1 - \langle|a_-|^2\rangle)E_0(k) = kB^2\gamma E_0(k), \quad (61)$$

where $\gamma \equiv 1 - \langle|a_-|^2\rangle$ is chosen to control the magnitude of the initial helicity. For any $\gamma \in [0,1]$, $\langle|a_-|^2\rangle = 1-\gamma$, giving the variance of a_- needed to generate the initial velocity field according to Eq. (60). The energy spectrum for given γ is

$$E(k) = \frac{1}{2}B^2(\langle|a_+|^2\rangle + \langle|a_-|^2\rangle)E_0(k) = \frac{1}{2}B^2(2-\gamma)E_0(k), \quad (62)$$

so $B=[2/(2-\gamma)]^{1/2}$ rescales the energy spectrum to $E_0(k)$. Correspondingly the helicity spectrum becomes

$$H(k) = \frac{\gamma}{2-\gamma}2kE_0(k). \quad (63)$$

For given k and $E_0(k)$, the helicity spectrum increases with γ. When $\gamma=1$, $H(k)=2kE_0(k)$, reaching the maximal spectral distribution for given energy spectrum $E_0(k)$ [31].

In all the simulations of decaying turbulence, γ is fixed to be one. In other words, the velocity field is always initialized with maximal helicity. $k_p=3$ and $u_0=0.4$, so that initially the integral length scale is estimated as $l_0=\pi/k_p \approx 1.047$ and the eddy turn-over time scale is $\tau_0=l_0/u_0 \approx 2.618$. For LES, 15 realizations are generated for each model. The results are averaged over the whole ensemble. Because in decaying turbulence the helicity and energy dissipation rates are not known *a priori*, the nonlocal helical model is not applicable. Therefore it is not investigated. For the DNS, resolutions of 512^3 are used.

The first parameter examined is the helicity decay rate. According to the previous theoretical analysis, the Smagorinsky model underpredicts the helicity dissipation rate, so the helicity decay rate predicted by the Smagorinsky model may be expected to be slower than the DNS value. Indeed, Fig. 10 shows slower decay for the Smagorinsky model than DNS, verifying the theoretical prediction. The decay rates predicted by the local helical model, Dyn-B, and Dyn-A models are successively closer to, albeit still lower than, the DNS value. The dynamic Smagorinsky and mixed nonlinear models yield results close to the Dyn-A model. Overall, the difference is quite small.

The helicity spectra are compared in Fig. 11. Because helicity is not positive definite, the helicity spectrum from DNS shows relatively large statistical fluctuations (due to machine time limitations, only one realization of helical DNS is available. For this reason also only data up to $4\tau_0$ are shown.)

Similar to the results in steady turbulence, the spectra calculated with the Dyn-A model and local model are dissipated more than those calculated with the Smagorinsky model at the highest wave-number end, while the Dyn-B model is less dissipative there. The local helical model predicts essentially the same spectra as the Smagorinsky model does at low wave-number range, where the Dyn-A and Dyn-B models predict faster decay. The differences between the dynamic Smagorinsky or the mixed nonlinear model and the Smagorinsky model are the same as those found for the energy spectrum in the nonhelical case [30] (e.g., closer prediction at the intermediate wave-number range, and the absence of pile-up at the cutoff wave-number in the spectrum predicted by the mixed nonlinear model).

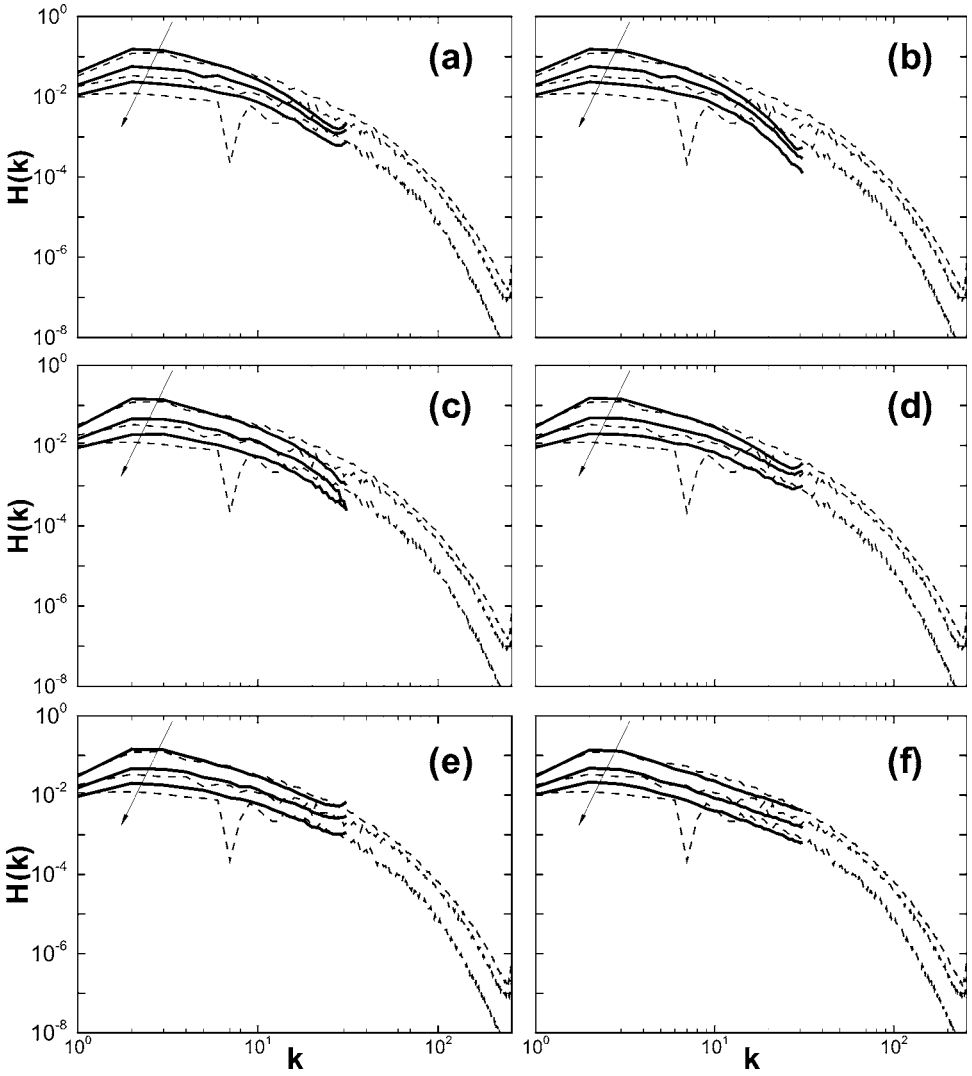

FIG. 11. The decay of the helicity spectrum. Line patterns are the same as in Fig. 10. Along the direction of the arrow, the times of decay are, respectively, $2\tau_0$, $3\tau_0$, and $4\tau_0$.

The fact that the helical model is more dissipative is consistent with the requirement of increasing the helicity dissipation rate according to the theoretical analysis based on the Kolmogorov-type spectrum; but from the figure it is also clear that the lower helicity decay rate predicted by the Smagorinsky model as compared with DNS is mainly due to the slow decay of helicity in the low wave-number modes. This deficiency is not improved by adding the helical term. Instead, the dynamic models predict higher decay rate for the helicity in the low wave-number region, as happened for energy spectrum observed previously [30]. Therefore present results suggest that it is mainly the dynamic procedure that helps improve slightly the prediction of helicity spectrum and helicity decay rate.

As shown with DNS data in [13], the energy cascade is suppressed by strong mean helicity in decaying helical turbulence. Therefore when the helicity is overpredicted by the Smagorinsky model as a result of the underestimation of helicity dissipation, one might expect that the energy cascade is suppressed excessively so that the energy decay rate is lower than it should be. On the other hand, the helical models, which predict higher SGS helicity dissipation rate, should predict higher energy decay rate than the Smagorinsky model. To test this conjecture numerically, we plot in Fig. 12 the energy decay predicted by DNS and the helical models as a function of time. The main observations are that the decay rates predicted by the Smagorinsky and the local helical models, which are essentially the same, are lower than the DNS value, and that the Dyn-A and Dyn-B models predict higher decay rates than the Smagorinsky model, giving closer result with DNS. However, comparing these results with the energy decay found in nonhelical turbulence [30], we can see that the difference between the Smagorinsky model and the DNS data is actually not bigger than in the nonhelical case. Therefore the Smagorinsky model has captured at least the major part of the suppressing effect of helicity on energy cascade.

Given the fact that the dynamic procedure already gives improved energy decay rate in nonhelical turbulence [30], the improvement of the dynamic models observed here might also be attributed to the improved prediction of energy, rather than helicity, statistics. The reason why the theoretical prediction is not observed may be that the theoretical arguments used in Sec. II assumed a Kolmogorov-type spectrum, while the actual spectrum calculated by the Smagorinsky model does not follow exactly Kolmogorov scaling.

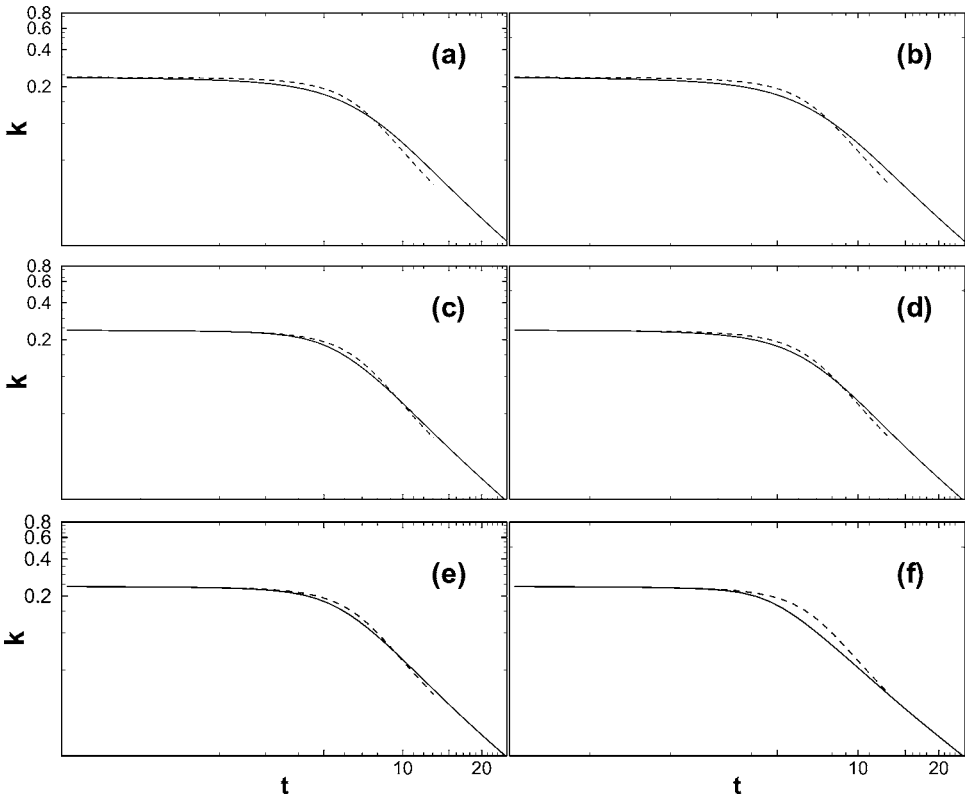

FIG. 12. The decay of mean kinetic energy. Line patterns are the same as in Fig. 10.

The evolution of energy spectra in decaying turbulence was also analyzed in the same fashion, and results (not shown) led to similar conclusions. Also examined was the case of rotating turbulence (with Rossby number down to Ro=0.1), in which the presence of helicity is known in general to affect energy decay rate. However, the differences between the various SGS models on the resolved statistics were negligible, even in the presence of strong rotation.

IV. CONCLUSIONS

The SGS dissipation of helicity and energy produced by the Smagorinsky model, the dynamic version of the Smagorinsky model, the mixed nonlinear model, and some proposed helical models has been investigated. By assuming a Kolmogorov spectrum, it is shown analytically that the Smagorinsky model underestimates the helicity dissipation by about 40%. This prediction is expected to hold asymptotically at very high Reynolds numbers under ideal conditions. To formulate models in which helicity dissipation can be prescribed directly, two two-term helical models are proposed. These are motivated by the form of the SGS helicity dissipation term in the equation of resolved helicity. The coefficients are determined either by simultaneous energy and helicity balance or by dynamic procedures. When devising the dynamic procedure, we also propose to use the Germano identity in the form of SGS force, in an effort to comply with the material frame indifferent requirement for the model coefficients. The nondynamic helical models are analyzed *a priori* and all the models are applied to the simulation of isotropic steady and decaying turbulence. It is shown that for most of the helical models the added term contributes a significant part to the helicity dissipation, while it does not much affect the energy dissipation. The decay rate of helicity in decaying helical turbulence is improved to some extent by the helical models. However, the overall effect of the added terms is small. In general, the dynamic models give better results, mainly because of their ability to predict more accurately the energy dissipation rates. In particular, the dynamic Smagorinsky and the dynamic mixed nonlinear model, which had in the past been proven to yield realistic energy dissipation rates, also yield improved helicity spectra. It is also found that the dynamic model derived from the Germano identity for SGS force is slightly more dissipative in energy than the traditional dynamic model, and the helical term is almost totally turned off by the dynamic procedure.

As a broad conclusion, we find that the model based on global helicity dissipation requirement is not very different from the standard dynamic Smagorinsky model, and current models (e.g., mixed nonlinear model) are able to yield reasonably good results.

ACKNOWLEDGMENT

The authors are grateful for support from the National Science Foundation through Grants CTS-0120317 and ITR-0428325.

[1] H. K. Moffatt and A. Tsinober, Annu. Rev. Fluid Mech. **24**, 281 (1992).
[2] A. Brissaud, U. Frisch, J. Leorat, M. Lesieur, and A. Mazure, Phys. Fluids **16**, 1366 (1973).
[3] J. C. André and M. Lesieur, J. Fluid Mech. **81**, 187 (1977).
[4] V. Borue and S. A. Orszag, Phys. Rev. E **55**, 7005 (1997).
[5] Q. Chen, S. Chen, G. L. Eyink, and D. D. Holm, Phys. Rev. Lett. **90**, 214503 (2003).
[6] R. H. Kraichnan, J. Fluid Mech. **59**, 745 (1973).
[7] H. K. Moffatt, J. Fluid Mech. **159**, 359 (1985).
[8] A. Tsinober and E. Levich, Phys. Lett. **99A**, 321 (1983).
[9] R. B. Pelz, V. Yakhot, S. A. Orszag, L. Shtilman, and E. Levich, Phys. Rev. Lett. **54**, 2505 (1985).
[10] M. M. Rogers and P. Moin, Phys. Fluids **30**, 2662 (1987).
[11] R. M. Kerr, Phys. Rev. Lett. **59**, 783 (1987).
[12] J. M. Wallace, J.-L. Balint, and L. Ong, Phys. Fluids A **4**, 2013 (1992).
[13] W. Polifke and L. Shtilman, Phys. Fluids A **1**, 2025 (1989).
[14] W.-S. Wu, D. K. Lilly, and R. M. Kerr, J. Atmos. Sci. **49**, 1800 (1992).
[15] C. G. Speziale, *Recent Advances in Engineering Science*, *Lecture Notes in Engineering*, edited by S. L. Koh and C. G. Speziale (Springer-Verlag, Berlin, 1989), Vol. 39, p. 50.
[16] D. K. Lilly, J. Atmos. Sci. **43**, 126 (1986).
[17] M. Lautenschlager, D. P. Eppel, and W. C. Thacker, Beitr. Phys. Atmos. **61**, 87 (1988).
[18] D. K. Lilly, *Proceedings of the IBM Scientific Computing Symposium on Environmental Sciences* (Yorktown Heights, NY, 1967), p. 195.
[19] M. Germano, U. Piomelli, P. Moin, and W. H. Cabot, Phys. Fluids A **3**, 1760 (1991).
[20] G. K. Batchelor, *The Theory of Homogeneous Turbulence* (Cambridge University Press, Cambridge, England, 1956).
[21] J.-J. Moreau, Acad. Sci., Paris, C. R. **252**, 2810 (1961).
[22] M. Lesieur, *Turbulence in Fluids* (Martinus Nijhoff Publishers, Dordrecht, 1987).
[23] S. Cerutti, C. Meneveau, and O. M. Knio, J. Fluid Mech. **421**, 307 (2000).
[24] Y. Li and C. Meneveau, Phys. Fluids **16**, 3483 (2004).
[25] C. Meneveau and J. Katz, Annu. Rev. Fluid Mech. **32**, 1 (2000).
[26] C. G. Speziale, Annu. Rev. Fluid Mech. **23**, 107 (1991).
[27] C. G. Speziale, Geophys. Astrophys. Fluid Dyn. **33**, 199 (1985).
[28] H. Kobayashi and Y. Shimomura, Phys. Fluids **13**, 2350 (2001).
[29] C. Meneveau and T. S. Lund, Phys. Fluids **9**, 3932 (1997).
[30] H. S. Kang, S. Chester, and C. Meneveau, J. Fluid Mech. **480**, 129 (2003).
[31] Q. Chen, S. Chen, and G. L. Eyink, Phys. Fluids **15**, 361 (2003).
[32] F. Waleffe, Phys. Fluids A **4**, 350 (1992).